Atmos. Chem. Phys. Discuss., 10, 8103–8134, 2010
www.atmos-chem-phys-discuss.net/10/8103/2010/

Atmospheric Chemistry and Physics Discussions

This discussion paper is/has been under review for the journal Atmospheric Chemistry and Physics (ACP). Please refer to the corresponding final paper in ACP if available.

Assessing the regional surface influence through Backward Lagrangian Dispersion Models for aircraft CO_2 vertical profiles observations in NE Spain

A. Font[1,2], **J.-A. Morguí**[1,2], **and X. Rodó**[1,3]

[1]Institut Català de Ciències del Clima, Dr. Trueta 203, 08005, Barcelona, Catalonia, Spain
[2]Laboratori de Recerca del Clima, Parc Científic de Barcelona, Universitat de Barcelona, Baldiri i Reixach, 4-6, Torre D, 08028, Barcelona, Catalonia, Spain
[3]Institució Catalana de Recerca i Estudis Avançats, Passeig Lluís Companys, 23, 08010, Barcelona, Catalonia, Spain

Received: 4 January 2010 – Accepted: 1 March 2010 – Published: 29 March 2010

Correspondence to: A. Font (afont@ic3.cat)

Published by Copernicus Publications on behalf of the European Geosciences Union.

Abstract

A weekly climatology for 2006 composed of 96-h-backward Lagrangian Particle Dispersion simulations is presented for nine aircraft sites measuring vertical profiles of atmospheric CO_2 mixing ratios along the 42° N parallel in NE Spain to assess the surface influence at a regional scale (10^2–10^3 km) at different altitudes in the vertical profile (600, 1200, 2500 and 4000 meters above the sea level, m a.s.l.). The Potential Surface Influence (PSI) area for the 96-h-backward simulations, defined as the air layer above ground with a thickness of 300 m, are reduced from the continental scale (~10^7 km^2) to the watershed one (~10^4 km^2), when a Residence Time Threshold Criteria (R_{ttc}) greater than 500 s is imposed for each grid cell. In addition, this regional restricted information is confined during 50 h before the arrival for simulations centered at 600 and 1200 m a.s.l. At higher altitudes (2500 and 4000 m a.s.l.), the regional surface influence is only recovered during spring and summer months. For simulations centered at 600 and 1200 m a.s.l. sites separated by ~60 km may overlap 20–50% of the regional surface influences whereas sites separated by ~350 km as such do not overlap. The overlap for sites separated by ~60 km decreases to 8–40% at higher altitudes (2500 and 4000 m a.s.l.). A dense network of sampling sites below 2200 m a.s.l. (whether aircraft sites or tall tower ones) guarantees an appropriate regional coverage to properly assess the dynamics of the regional carbon cycle at a watershed scale (10^2–10^3 km length scale).

1 Introduction

Atmospheric measurements show that the CO_2 concentration in the atmosphere is currently ~387 ppmv; but this global average must be downscaled to know the regional distribution of CO_2 emissions (Marquis and Tans, 2008). Improving our understanding of the carbon cycle at various spatial and temporal scales will require the integration of multiple, complementary and independent methods used by different research

ACPD

10, 8103–8134, 2010

communities (Canadell et al., 2000). The assessment of CO_2 surface fluxes is mainly available at two spatial scales: the local and the global scales (Lafont et al., 2002). Local fluxes are inferred by eddy covariance systems placed mainly on forest and/or grass lands (Baldocchi et al., 2001). This methodology provides estimates of carbon fluxes at fine spatial scales (10^1–10^2 km). Global fluxes are based instead on atmospheric inverse transport studies based on CO_2 measurements over large areas, inverse numerical methods and satellite data (Ciais et al., 1995; Fan et al., 1998; Bousquet et al., 1999; Gurney et al., 2002, 2008; Peters et al., 2009). But global inversions do not provide much spatial resolution nor do they have the potential to increase the current understanding of the terrestrial processes, responsible for the future control of fluxes (Canadell et al., 2000). The CO_2 concentration over continents shows a large variability resulting from the high variability of surface fluxes and they vary spatially across the landscape in close relation to vegetation types and conditions (Gerbig et al., 2003a; Sarrat et al., 2007a; Choi et al., 2008); as well as in time due to the sign reversing of biospheric fluxes between night (respiration) and day (photosynthesis), and to the strong daily mixing within the planetary boundary layer (Gloor et al., 2001; Lafont et al., 2002; Gerbig et al., 2008; Denning et al., 2008). In addition, CO_2 variability is also linked to the synoptic and mesoscale changes in meteorological conditions (Sidorov et al., 2002; Shashkov et al., 2007). The interpretation of the mixing ratios is linked then to the knowledge of the surface fluxes around the measurement sites and at a regional scale (Lin et al., 2004). Currently, high resolution mesoscale models have been used to cope with the variability in the atmospheric boundary layer over land at a regional scale. Mesoscale models may provide a more appropriate transport of CO_2 and other trace gases at high spatial resolution but uncertainties are still large (Sarrat et al., 2007b). Another way to cope with changes in regional fluxes is analyzing vertical profiles of concentration; either collected at one location from tall towers (i.e. Bakwin et al., 1995, 1998) or from vertical sampling by aircraft (Wofsy et al., 1988; Lloyd et al., 2002; Schmitgen et al., 2004; Martins et al., 2009; Sarrat et al., 2009). These methods are based on the idea that trace gas concentration in the air at greater altitudes above

the ground is influenced by a longer upwind fetch, thus being representative of a larger area than air close to the ground (Tans et al., 1996). Further, measurements of vertical profiles allow the determination of mixing heights to finally reduce the uncertainties in simulated vertical mixing (Gerbig et al., 2009). The footprint concept around measurement sites has been widely used to quantify from where and to which extent fluxes within the surrounding areas influence trace gas observations (Gloor et al., 2001). The footprint concept is thus a representation of the sensitivity of mixing ratios at the measurement locations to upstream fluxes at prior times (Gerbig et al., 2009). It varies with height, but also with the wind direction, meteorological conditions (stability) and the magnitude of the CO_2 fluxes (Rannik et al., 2000; Aubinet et al., 2001).

The footprint area or the Potential Surface Influence (PSI) of nine aircraft sites in NE Spain situated along the 42° N parallel at different altitudes (600, 1200, 2500 and 4000 m above sea level, m a.s.l.) is calculated to assess the regional upwind influence of CO_2 measurements. The regional scale of 10^2 and 10^3 km length-scale on a seasonal basis is addressed by the Lagrangian Particle Dispersion Model (LPDM) FLEXPART in backward mode. The time and altitude influence scale and the percentage of the spatial overlapping of the PSI between aircraft sites are analyzed to draw conclusions about the CO_2 sampling strategy.

2 Methods

2.1 The ICARO-II aircraft surveys

The aircraft sites belong to the aircraft network ICARO-II in Spain are sampled following the Crown Aircraft Sampling (CAS) described previously in Font et al. (2008). CAS samples continuously CO_2 mixing ratios in the vertexes of a prism, separated ~60 km, integrating vertical profiles from 600 to 2500 and 4000 m a.s.l. with horizontal transects at 600 and 1200 m a.s.l. Three regions are sampled following CAS in NE Spain (Fig. 1): La Muela crown, Linyola crown and Ullastret crown. The vertexes in La Muela crown

are La Muela (LMU, 41.60° N 1.1° W), Tarazona (TRZ, 41.84° N 1.52° W) and Egea de los Caballeros (EGA, 42.12° N 1.12° W); for Linyola crown, vertexes are Linyola (LIN, 41.71° N 0.88° E), Mequinensa's Dam (MEQ, 41.35° N 0.28° E) and Binéfar (BIN, 41.84° N 0.27° E); for Ullastret crown, Ullastret (ULL, 42.00° N 3.02° E) and two maritime sites over the Mediterranean Sea: one situated at 42° N 4.5° E (MR1); the other located at 41.50° N 3.50° E (MR2). The median distances between crowns are 150 km (LMU-LIN crowns) and 280 km (LIN-ULL crowns).

2.2 LPDM model

The Lagrangian Particle Dispersion Models (LPDMs) are well-suited to delineate contributions from upwind source regions (Blanchard, 1999) at different spatial scales. FLEXPART model simulates long-range and mesoscale transport, diffusion, dry and wet deposition, and radioactive decay of tracers released from point, line, area or volume sources (Stohl et al., 2005). The model parameterizes turbulence in the boundary layer and in the free troposphere by solving Langevin equations (Stohl and Thompson, 1999). LPDM backward simulations replace the traditional backward trajectory calculations as they account not only advection but also turbulence, convection and large-scale advection (Stohl et al., 2002; Seibert and Frank, 2004). The LPDM FLEXPART is used here to assess the upwind source regions of nine CO_2 vertical profiling sites (LMU, TRZ and EGA; LIN, MEQ and BIN; ULL, MR1 and MR2) at four different altitudes (height of release points: 600, 1200, 2500 and 4000 m a.s.l.). FLEXPART is driven by the global model-level data NOAA-NCEP-GFS (National Oceanic and Atmospheric Administration – National Centers for Environmental Prediction – Global Forecast System) with a horizontal resolution of 1°×1° and 26 vertical layers and a time resolution of 3 h (analyses at 00:00, 06:00, 12:00, 18:00 UT; forecasts at 03:00, 09:00, 15:00 and 21:00 UT). Ten thousand particles are released at 12:00 UT and transported four days back in time by the resolved winds and by parameterized subgrid and convection motions. The release points are defined as small boxes round the measurement sites with dimensions 0.01°×0.01°×10 m. The model output (120×110×16 grids with a

horizontal resolution of 0.5°×0.5°; 16 vertical levels from ground up to 3000 m above ground level (m a.g.l.); temporal resolution of 3 h) consists of a response function related to the particles residence time (R_t) in each grid. The size of the output grid cells is related to the scale of distances between two closest measurement sites. No removal processes are considered in the simulations. It is assumed that the R_t in one grid cell is proportional to the source contribution to the mixing ratio at the measurement site.

A weekly based climatology of LPDM simulations for the nine aircraft sites at four different altitudes (600, 1200, 2500 and 4000 m a.s.l.) is presented. The weekly climatology is based in 51 days for 2006. Summing up, a total of 1836 simulations (459 simulations for each altitude) build up the 2006 climatology analyzed in this study.

3 Results

The distribution of air masses in the lower troposphere (0 up to 3000 m a.g.l.) and the assessment of the regional upwind PSI area (10^2–10^3 km length scale) of aircraft measurements sites in a climatology basis are examined in Sect. 3.1. In Sect. 3.2, the spatial relations of the PSI of the different sites belonging to the Spanish network are studied. Abbreviations used are: DJF for December, January and February; MAM for March April and May; JJA for June, July and August; SON for September, October and November.

3.1 Upwind sources for aircraft measurement sites

The upwind source region for each of the four release points in profiles is studied. Five layers in the model output lower troposphere (0–3000 m a.g.l.) are defined: from 0 to 300 m (L1); from 301 to 800 (L2); from 801 to 1200 (L3); from 1201 to 3000 (L4); and above 3000 m a.g.l. (L5; out of the model output domain). The first layer is considered to be within the Planetary Boundary Layer (PBL); then, closely influenced

by the terrestrial or marine surface carbon fluxes. Conversely, the last two layers (L4 and L5) are considered to belong to the Free Troposphere (FT). L2 and L3 stay in a middle zone situated either in the PBL, the Entrainment Zone (EZ) or the FT, depending both on the time of the day and on the weather conditions. Figure 2a summarizes the annual percentage of air masses residence time in each layer in a 3 h time step. Usually, air masses reside more time in L1 as release points or simulations are lower in the profile.

At 600 m a.s.l., the residence time in L1 is ∼30% at the beginning of simulations, decreasing to 10% at the very end of them. For high altitudes, air masses residence time in L1 is very short: ∼5% at 2500 m a.s.l. and less than 1.5% at 4000 m a.s.l. all along the 96 h simulations. For the 4000 m a.s.l. release point, air masses are mainly encountered outside the output domain (L5) most of the time (∼85%).

Seasonally, the percentage of R_t in L1 is higher during winter and autumn for simulations centered at 600 m a.s.l. For the first three hours of simulation, air masses remain more than 40% of the time (DJF) and 35% (SON) in L1 and this ratio decreases at ∼20% for MAM and JJA. At 1200 m a.s.l., no seasonal pattern is retrieved as air masses resides ∼20% in L1 during all seasons. For simulations starting at 2500 and at 4000 m a.s.l., percentage of R_t in L1 is higher during warm months (reaching percentages of 10% and 5%, respectively) rather than cold ones (less than 5% and 2%, respectively).

The distribution of the percentage of R_t in L1 is related to the seasonality of atmospheric stability. During warm months, the convective boundary layer enhances intensive downward and upward motions leading to a well-mixed PBL. Convection acts as a scattering factor for particles, distributing them randomly in the PBL whereas during winter and autumn months, inversions take place more often suppressing vertical transport near the surface and within the PBL. The vertical transfer of air masses in summer is more than a factor of 5 faster than in winter (Liu et al., 1984). During winter and autumn, the higher frequency of fronts and the uplift motions of air associated to them enhance the transfer of particles from lower layers up to higher ones. The transfer

of particles from L5 or L4 down to other layers during warm months is associated to subsidence processes associated to anticyclonic weather.

L1 was defined to encompass the Potential Surface Influence (PSI) concept in order to assess the upwind surface source region for atmospheric CO_2 mixing ratios. The PSI is the 300 m thickness layer adjacent to the ground where air masses have probably remained before arriving at the measurement site. The thickness of PSI is chosen as it is within the Planetary Boundary Layer (PBL) most of the time and it is high enough to allow large number of particles to be sampled (Stohl et al., 2003). In this study, the PSI (L1) was characterized in size and shape as a property function of the air mass transport, and it is independent of the intensity and amount of surface fluxes. The mean annual residence time of air masses in the PSI (R_t-PSI) is 14%, 11%, 4.3% and 1.1% of the total simulation time (96 h) for the release points centered at 600, 1200, 2500 and 4000 m a.s.l., respectively. There is an abrupt change in the annual mean R_t-PSI depending on whether the particle's release altitude is above or below the PBL height. This discontinuity is related to the fact that air masses from the FT remain there unless subsidence processes allow mixing down. Consequently, CO_2 mixing ratios above the PBL are less influenced by the short-term CO_2 changes due to surface sources and sinks.

The area occupied by PSI in km^2 (PSI area) is larger as simulations started lower in the vertical profile (Fig. 2b). Hence, the annual PSI area for simulations started at 600 m a.s.l. is $(2.3\pm1.2)\times10^6$ km^2 whereas at 4000 m a.s.l. is $(1.1\pm1.2)\times10^6$ km^2. There is a mean reduction of 53% of the PSI area from 600 to 4000 m a.s.l. There is also a seasonal variability as PSI areas retrieved during MAM, JJA and SON are larger, $(2.5\pm1.1)\times10^6$ km^2; $(2.2\pm0.9)\times10^6$ km^2 and $(2.4\pm1.5)\times10^6$ km^2, for simulations centered at 600 m a.s.l.; whereas they are smaller during DJF, $(1.9\pm1.1)\times10^6$ km^2 at the same altitude. The reduction of PSI area for higher release points is 68%, 60%, 41% and 46% at DJF, MAM, JJA and SON, respectively.

A Residence Time Threshold Criteria (R_{ttc}) are applied with the aim of assessing the regional scale (10^2–10^3 km length scale) of upwind surface source regions of aircraft

ACPD
10, 8103–8134, 2010

sites. Under a theoretical assumption of a homogenous distribution of the total R_t in the PSI grid cells, it could be found that for a R_t of 500 s for each grid cell, the area covered is within the 10^2 km scale. As for the 60 s case, the scale of the PSI coverage is 10^3 km.

When R_{ttc} are applied to the overall PSI, there is a mean reduction of 95.4±3.7% of the PSI area (Fig. 2b). As more restrictive the criterion is a larger reduction is obtained: 99.2±0.7% (500-s-R_{ttc}); 97.4±1.8% (200-s-R_{ttc}); 94.3±3.2% (100-s-R_{ttc}) and 90.1±4.5% (60-s-R_{ttc}). Moreover, the PSI area reduction is larger as simulations start at higher altitudes in the profile. Then, a reduction of 98.6±1.5% is accounted at 4000 m a.s.l. while 92.9±4.7% at 600 m a.s.l. No seasonal differences in the reduction of the PSI area are found. The order of magnitude of PSI area shrinks from the European continent one ($\sim 1\times10^7$ km^2) to the Ebre watershed scale (8.6×10^4 km^2) for 500-s-R_{ttc}. Whichever restriction is used, the ground influence is almost lost at 2500 m a.s.l., thus confining the regional surface influence (10^2–10^3 km length scale) in the first 1200 m of the vertical profile. Then, CO_2 measurements at higher altitudes are supposed to belong to a well-mixed latitudinal concentration not influenced by the short-term local and regional surface processes, and are frequently used as boundary conditions (Gerbig et al., 2003b).

The annual mean number of PSI grid cells with R_t of 500, 200, 100 and 60 s are tracked back in time for simulations at 600, 1200, 2500 and 4000 m a.s.l. (Fig. 2c). For simulations centered at 600, 1200 or 2500 m a.s.l., the 10^3 km length-scale information is lost after the 50 h of simulation. Thus, the surface regional information is only confined in two diurnal cycles before arriving at the measurement site. At 4000 m a.s.l., regional influence is scarcely recovered. These results highlight that simulation-times up to 50 h are enough for studies scoping the assessment of upwind surface regional influence at 10^2–10^3 km horizontal scales.

The application of the R_{ttc} underestimates the CO_2 mixing ratio from advection upstream to measurements sites. A quantification of the "missed" CO_2 mixing ratio is accounted for by evaluating the minimal R_t in the PSI needed to detect changes in the

ACPD
10, 8103–8134, 2010

CO_2 mixing ratio due to surface fluxes. A marginal change in the atmospheric CO_2 mixing ratio depends first on the precision of the analyzer used; and second, on the intensity of surface fluxes. Different precision numbers are considered, ranging from 0.05 ppmv, for high precision atmospheric CO_2 analyzers to ~0.25 ppmv, the typical precision of airborne systems (Font et al., 2008). The intensity of fluxes is taken from the yearly mean maxima, the yearly mean minima and the yearly mean of daily averages of 3-hourly fluxes from the global assimilation system CarbonTracker-Europe (Peters et al., 2007, 2009) for Europe in 2006. It results into a mean daily maxima flux of 16.3 µmol CO_2/m^2 s, a mean daily minima flux of −28.2 µmol CO_2/m^2 s; and a mean daily average of 0.1 µmol CO_2/m^2 s. The characterization of the response of the R_t vs. the PSI area is shown in Fig. 3a. The R_t in the PSI needed to detect changes in the measured concentration with aircraft instrumentation ranges from ~100 up to ~200 s when yearly mean daily maxima and minima fluxes values are considered. Large R_t, greater than 7500 s, are needed to detect changes in measured CO_2 when the daily mean is considered (0.1 µmol CO_2/m^2 s). Thus, whichever R_{ttc} applied (500 and 60 s), it does not miscalculate the contribution of one single PSI grid cell as very much larger R_t are needed to detect changes in the CO_2 concentration due to surface fluxes in airborne analyzers.

Although extremely large residence time is needed to detect changes induced by one single grid cell, the addition of the contribution of a large number of cells with low R_t values may lead to significant changes into measured CO_2 mixing ratios. In order to evaluate this effect, a similar approach is taken. It is estimated the area formed by grid cells having R_t of 59, 10 and 1 s required to detect changes in the CO_2 mixing ratio by analyzers with different mean precision (0.05, 0.1 and 0.25 ppmv). For a surface having a homogenous flux of 0.1 µmol CO_2/m^2 s it would be needed a PSI area larger than the Danube basin (>10^5 km^2) to detect changes in the CO_2 concentration; and PSI area larger than the Ebre basin (10^4 km^2) would be required for grid cells having R_t less than 10 s with surface fluxes of 16.3 and −28.2 µmol CO_2/m^2 s (Fig. 3b). For R_t of 59 s, the PSI area required is about 10^3 km^2. Consequently, very large R_t and wide

ACPD
10, 8103–8134, 2010

PSI areas with R_t lower than 10 s are needed to detect CO_2 mixing ratios changes in the measurement sites. If R_{ttc} are applied, there is no detectable influence of the missed CO_2 mixing ratio according to the instrumental uncertainty of aircraft analysis.

Rejected PSI grid cells, that is, those ones having R_t<60 s, are attributed to external regional surface influence (larger horizontal scales than 10^3 km); and the PSI grid cells with R_t>60 s are all considered to belong to the internal regional surface influence. On the assumption that all PSI grid cells has the same surface flux, the 500-s-PSI (the 10^2 km region around the measurement sites) gather ~40% of total advected upstream CO_2 concentration at 600 m a.s.l.; ~30% at 1200 m a.s.l.; ~9.5% at 2500 m a.s.l. and ~1.5% at 4000 m a.s.l. Similarly, the 60-s-PSI (the 10^3 km region around the measurement sites) accounts for ~80% at 600 m a.s.l, ~73% at 1200 m a.s.l.; ~43% at 2500 m a.s.l. and ~20% at 4000 m a.s.l. (Fig. 4). Then, the CO_2 contribution from the external regional surface influence far from 10^2–10^3 km represents ~20%, ~27%, ~57% and ~80% at 600, 1200, 2500 and 4000 m a.s.l., respectively. As expected, going up in the vertical profile, the total external regional surface CO_2 contribution advected upstream is larger than at low levels. At ~2200 m a.s.l., the CO_2 regional surface contribution equals the external one. Measurements done below 2200 m a.s.l. are needed for a good characterization of the surface fluxes in the immediate proximity of observatories measuring CO_2 atmospheric concentrations.

PSI spatial patterns are examined through Principal Component Analysis (PCA). PCA, known as eigenvector analysis or as empirical orthogonal function analysis, has been used in studies to determine the spatial pattern of meteorological variables (Overland and Preisendorfer, 1982) or air pollution (Ashbaugh et al., 1984). PCA reduces the dimensions of the original data (p) to a smaller number of independent new variables m (m<p) that are a linear combination of the former ones and are ordered by the fraction of original variance retained. The result is the definition of new variables or principal components (m or PC). PCA analysis of the PSI results in the separation of PSI grid cells depending on the synoptic situation. For each of the 9 aircraft sites in NE Spain (Fig. 1), the R_t of PSI-500-s grid cells for simulations centered at

600 m a.s.l. (observations) for 51 simulations for 2006 (variables) configured the original PCA matrix with only those grid cells appearing at least in one of the 51 simulations. Therefore, the original PCA matrix is actually an absence/presence one. The plot of the geographical distribution of the PSI values from each of the reduced axes from PCA analysis (PC1 and PC2) is shown in Fig. 5 and it represents the "footprint" of emission sources (Dorđjević et al., 2005; Huang et al., 2009). On the whole, PC1 identifies the closest surroundings around each aircraft measurement site whereas PC2 distinguishes the main wind directions, both in accordance with the topographic configuration around each measurement site. PC2 show a dipole distribution as it distinguishes different weather situations. PC1 and PC2 together gather ~75% of the original variance of the data set. The variance explained by each axis is different for the continental than for the maritime sites. PC1 explains 51.3±12.3% of the original variance in continental sites, but it only retains 23.3±1.4% of the original variance for the maritime crown sites (ULL, MR1 and MR2). For the continental sites, PC1 identifies the Ebre watershed influence. For the maritime sites, the PC1 identifies the Mediterranean Catalan coastline (ULL), the north east of the Balearic Island and the east Algerian Basin in the Mediterranean Sea (MR1) and the Balearic Sea (MR2). PC2 distinguishes between synoptic situations linked to the main wind directions. Incompatible weather situations are more steeped in continental sites as topography modulates the main wind channels. Conversely, topography is more diluted in maritime sites as it is shown by the low variance explained by each PC. PC2 separates N against W weather situations for BIN and LIN; NW against S for EGA, LMU and MEQ; NW against N situations for TRZ; N continental against Balearic Sea influence for ULL; local winds against Corsica coast originated ones for MR1; and continental against Balearic sea winds for MR2.

Similar results are obtained in carrying out PCA for PSI-60-s grid cells to all aircraft sites for the 51 simulations of 2006. The variability explained by PC1 and PC2 is alike. In order to check the altitude influence, PCA were also carried out for PSI for simulations centered at 1200, 2500 and 4000 m a.s.l. Whereas similar patterns are retrieved for 1200 and for 600 m a.s.l., incongruent spatial patterns are retrieved for

ACPD
10, 8103–8134, 2010

2500 and 4000 m a.s.l. This is expected as neither 10^2 nor 10^3 km length-scales are well retrieved at high altitudes of the vertical profile. PCA is an alternative way to calculate the average footprint of a measurement site to those methods based in the integration of footprint functions (i.e. Matross et al., 2006) as it also keeps synoptic information.

3.2 Spatial PSI relationships between crown sites of the aircraft measurements ICARO program

As explained in Sect. 2.1, the Crown Atmospheric Sampling (CAS) used in this study samples three sites placed in the vertexes of a 60-km-side triangular area (LMU-TRZ-EGA; LIN-MEQ-BIN and ULL-MR1-MR2). The percentage of PSI-overlapping between sites belonging to the same crown is calculated and from now on is called intra-crown comparison. The mean annual intra-crown PSI-overlapping percentage is ∼90% for LMU-TRZ-EGA and LIN-MEQ-BIN, and ∼80% for the ULL-MR1-MR2 crown, for simulations centered at low altitudes, and decreases up in the vertical profile: ∼70% for continental crowns, and ∼60% for the maritime one. No remarkable differences of annual PSI-overlapping percentage are found between seasons at low altitudes (600 and 1200 m a.s.l.) whereas at higher ones (2500 and 4000 m a.s.l.) seasonal differences brought out: less overlapping during the cold season (DJF) and more during warm season (MAM and JJA) are observed.

Applying a 500 s R_t threshold, there is a reduction of the mean annual PSI-overlapping percentage (Table 1): at 600 m a.s.l. it is ∼50% (LMU crown) and ∼45% (LIN crown); at 1200 m a.s.l., percentages are similar: ∼46% and ∼43%, respectively. Therefore, measurements carried out in sites belonging to the same crown share between 40 and 50% of 10^2 km-length-scale surface information when sampled below 1200 m a.s.l. The PSI-overlapping percentage above 2500 m a.s.l. is lower, ranging from 8% to 38% depending on the crown.

ACPD
10, 8103–8134, 2010

Although continental crowns share in average ~45% of the 10^2 km surface regional information at lower levels of the profile, discrepancies in the intra-crown comparison show up. The simulation started on 7 February 2006 at 12:00 UT centered at 600 m a.s.l. for LIN-MEQ-BIN is an interesting example and is displayed in Fig. 6a. Even though the intra-crown comparison shares 40% of the upwind surface region, each site gleans different 10^2 km regional information. Different transversal Pyrenean valleys are crossed by air masses before reaching each respective measurement site. Air masses arriving at LIN with N component cross the Pyrenees by the Pallaresa valley. Conversely, air masses arriving at MEQ cross the Pyrenees by a more western valley, gathering the influence from the upper Ebre watershed before reaching the measurement site.

Intra-crown PSI-overlapping percentage between sites of the maritime crown is lower compared to the continental ones. Both larger distance between vertexes (~130 km between ULL and MR1; ~100 km between MR1 and MR2; and ~68 km between MR2 and ULL) and no geographical neither topography disruptions modifying air masses dispersion (except coast and islands), explain the low overlapping.

For the inter-crown comparison (between sites belonging to different crowns), the Sorensen's Quotient of Similarity (*Q/S*) is used in Eq. (1) as expressed in Kobayashi (1987).

$$Q/S = \frac{2j}{(a+b)} \cdot 100 \quad (1)$$

where *a* and *b* are the PSI area for each site, and *j* is the PSI common area shared by both sites. For the lowest level computed (600 m a.s.l.), without R_{ttc} applied, the quotient of similarity ranges from 70 to 50% values depending on the distance between sites compared: as closer as sites are located, higher *Q/S* is obtained. When the 500-s-R_{ttc} is used (Table 2), the annual *Q/S* quotient is reduced by a factor of 10 for sites situated 150 km-away at either 600 or 1200 m a.s.l., with *Q/S* values ranging from 5 to 11% (LIN-ULL; LMU-LIN); and by a factor of 100 for sites situated 350 km

ACPD
10, 8103–8134, 2010

away, with *Q/S* values of 0.6% (LMU-ULL). At 2500 m a.s.l., very low *Q/S* values are attained (less than 3% for LMU-LIN and LIN-ULL; and 0.4% for LMU-ULL). Seasonally, large *Q/S* values are globally found during winter (DJF) whereas low values are registered during summer (JJA). As a consequence, more local influence is gathered by CO_2 measurements during warm months than in winter. The sort-term variability of the CO_2 concentration during warm months is determined by local meteorological conditions such as the depth of the boundary layer (Eneroth et al., 2003). Conversely, in winter, PSI is more influenced by large-synoptical scale processes, thus, enhancing large dispersion of PSI.

The 10^2 km regional surface information shared by different aircraft sites decrease as far they are situated. From pair-by-pair site calculation of the mean annual PSI-overlapping percentage for 500-s-PSI at 600 m a.s.l., the decrease follows an exponential function of distance (Fig. 7). Sites located 60 km away from each other (intra-crown comparison) share ~40% of the upstream regional surface influence; sites separated 150 km and 350 km (inter-crown comparison), only share 13% and 1%, respectively.

4 Discussion

Results reported in Sect. 3 have direct impact on the design of observational network of sites measuring atmospheric CO_2 concentration. Intensive sampling at altitudes lower than 2200 m a.s.l. is needed to quantify the regional CO_2 surface fluxes. The lowest levels of vertical profiles contain most of the regional CO_2 surface fluxes contribution. Moreover, a single measurement at 4000 m a.s.l. every 10^2–10^3 km is enough to measure the free troposphere CO_2 concentration not influenced directly by short-term surface regional processes. These results strengthen the CAS as a properly-designed sampling method to quantify CO_2 regional surface fluxes at 42° N in airborne platforms. Intensive sampling is accomplished below 2200 m a.s.l. (horizontal transects at 600 and 1200 m a.s.l.; repeated vertical profiles from 600 to 2500 m a.s.l.), reaching the FT CO_2 concentration by the profile up to 4000 m a.s.l. over only one vertex of

ACPD
10, 8103–8134, 2010

each crown. Atmospheric research flights implemented in regions with different topography configuration may experience different percentages of the regional and external surface contribution at each altitude.

Approximately 40% of the surface influence at levels below 2200 m a.s.l. in the profiles is confined in the 10^2 km regional/local scale. The dominance of the surrounding field contributions to daytime mixing ratios of CO_2 for inversion studies causes that a small bias in the assumed flux in the near field can bring a large bias in the modeled mixing ratio when only one measurement site is considered (Gerbig et al., 2009). A compensating effect rises when using multiple sites in a network: since a local bias in fluxes at one measurement location is a far-field small scale bias for other site, resulting errors are expected to be uncorrelated between different sites (Gerbig et al., 2009). Aircraft data and/or tall tower measurements with overlapping footprints in both surface area and vegetation class are needed to provide reliable regional CO_2 budgets (Matross et al., 2006). Differential overlapping coincidences within a network of measurement sites (as presented in this study) represent independent observations containing the same CO_2 regional surface flux information.

Furthermore, the discrepancies of the PSI-overlapping between sites (as seen in whether inter-crown and intra-crown comparisons in Sect. 3.2) keep the signals of the regional heterogeneity of land-atmospheric fluxes within one grid of the usual atmospheric inversion models. The resolution of the models lay between 5°×3.75° (inter-crown comparison distance) and 0.5°×0.5° (intra-crown comparison) resolution (Geels et al., 2007).

5 Conclusions

A weekly climatology composed of 96-h backward LPDM simulations has been presented for nine aircraft sites measuring CO_2 vertical profiles in NE of Spain. The Potential Surface Influence (PSI) for each of the nine sites is estimated. The importance of the application of Residence Time Threshold Criteria (R_{ttc}) in the retroplumes is

highlighted. Without the threshold, wide retroplumes with PSI grid cells with less than the required diffusive mixing time does not provide information about the upstream surface regional influence. Thresholds of 500 s and 60 s appear to be a useful methodology to identify those regions that contain regional information at 10^2 and 10^3 km length-scale, respectively. The application of R_{ttc} allows the shrinkage of roughly 95% of the PSI area, passing from the continental scale ($\sim 10^7$ km^2) to the regional scale ($\sim 10^4$ km^2). The application of R_{ttc} also marks out the 10^2–10^3 km regional surface influence along the air column. At high altitudes of the vertical profile (2500 and 4000 m a.s.l.), the surface influence is almost reduced to zero; consequently, CO_2 mixing ratios at these heights are related to the concentration of well-mixed latitudinal air masses that are not influenced by the short-term surface fluxes. The information related to the 10^3 km processes is caught within the first 50 hours of simulation, gathering both the diurnal radiation effect from the vegetation (photosynthesis/respiration diurnal cycle) and the structure of the low atmosphere (boundary layer diurnal evolution). This fact also points that no longer backward simulations are required to retrieve the regional information of CO_2 surface fluxes. The information related to the 10^2 km processes is mostly lost after the first 3 h of simulation, extended to 12 h in winter simulations due to the vertical stability that prevent air masses to disperse.

The PSI-500-s grid cells of each of the nine aircraft sites are classified depending on the weather situation determined by a PCA applied to a presence/absence matrix of PSI-500-s grid cells with R_t higher than 500 s. This analysis shows up to be a useful tool to identify spatial patterns of the upwind regional influence of the aircraft measurements depending on the synoptic situations (Fig. 5). The same analysis applied at high altitudes of the vertical profile (2500 and 4000 m a.s.l.) shows that measurements at these altitudes are lacked of upstream regional surface influence (10^2 km) and they belong to a well-mixed latitudinal concentration. Thus, CO_2 mixing ratios at ~2200 m a.s.l. still retrieve the regional surface fluxes whereas this is lost at higher altitudes of the vertical profile. Intensive sampling below this altitude is required to cope with the regional surface fluxes at 10^2 and 10^3 km length scale.

At low altitudes of the vertical profile (600 and 1200 m a.s.l.) sites separated 60 km (intra-crown comparison) share 50% (continental sites) and 25% (maritime sites) of the regional surface influence. At high altitudes (above 2200 m a.s.l.), the overlapping for the intra-crown comparison is lower than 40%. Sites sampled below 2500 m a.s.l. and separated 150 km share 10% of the regional surface influence. The shared surface information is null for sites 350 km apart. No regional surface information is either retrieved or shared between sites 150 km distant above 2500 m a.s.l. An intensive network of sites measuring CO_2 mixing ratios below 2200 m asl with overlapping PSI will increase the ability to assess the CO_2 regional carbon budget.

Acknowledgements. We would like to thank all the people who make possible the Aircraft Measurement Program in Spain, especially M. A. Rodríguez, I. Pouchet and the crew of Top Fly, Sunfly and A. Lapetra. The authors want also to thank to the NOAA-ESRL-GMD Research Group and especially to A. Hirsch, G. Pétron and C. Sweeny for the discussion on FLEXPART model. This research was funded by the Spanish Ministry of Education and Science (project REN2003-06089 and GL12398).

References

Ashbaugh, L. L., Myrup, L. O., and Flocchinim, R. G.: A principal component analysis of sulfur concentrations in the western United States, Atmos. Environ., 18, 783–791, 1984.

Aubinet, M., Chermanne, B., Vandenhaute, M., Longdoz, B., Yernaux, M., and Laitat, E.: Long term carbon dioxide exchange above a mixed forest in the Belgian Ardennes, Agr. Forest Meteorol., 108, 293–315, 2001.

Bakwin, P. S., Tans, P. P., Zhao, C., Ussler, W., and Quesnell, E.: Measurements of carbon dioxide on a very tall tower, Tellus, 47B, 535–547, 1995.

Bakwin, P. S., Tans, P. P., Hurst, D. F., and Zhao, C.: Measurements of carbon dioxide on very tall towers: results of the NOAA/CMDL programa, Tellus, 50B, 401–415, 1998.

Baldocchi, D., Falge, E., Gu, L., Olson, R., Hollinger, D., Running, S., Anthoni, P., Bernhofer, C., Davis, K., Evans, R., Fuentes, J., Goldstein, A., Katul, G., Law, B., Lee, X., Malhi, Y., Meyers, T., Munger, W., Oechel, W., Paw, U. K. T., Pilegaard, K., Schmid, H. P., Valentini, R., Verma, S., Vesala, T., Wilson, K., and Wofsy, S.: FLUXNET: A new tool to study the temporal and

spatial variability of ecosystem – scale carbon dioxide, water vapor and energy flux densities, B. Am. Meteorol. Soc., 82(11), 2415–2434, 2001.

Blanchard, C. L.: Methods for attributing ambient air pollutants to emission source, Annu. Rev. Energ. Env., 24, 329–365, 1999.

Bousquet, P., Ciais, P., Peylin, P., Ramonet, M., and Monfray, M.: Inverse modeling of annual atmospheric CO_2 sources and sinks, 1. Method and control inversion, J. Geophys. Res., 104(D21), 26161–26178, 1999.

Canadell, J. G., Mooney, H. A., Baldocchi, D. D., Berry, J. A., Ehleringer, J. R., Field, C. B., Gower, S. T., Hollinger, D. Y., Hunt, J. E., Jackson, R. B., Running, S. W., Shaver, G. R., Steffen, W., Trumbore, S. E., Valentini, R., and Bond, B. Y.: Carbon metabolism of the terrestrial biosphere: a multitechnique approach for improved understanding, Ecosystems, 3, 115–130, 2000.

Ciais, P., Tans, P. P., Trolier, M., White, J. W. C., and Francey, R. J.: A Large Northern Hemisphere Terrestrial CO_2 Sink Indicated by the $^{13}C/^{12}C$ Ratio of Atmospheric CO_2, Science, 269, 1098–1102, doi:10.1126/science.269.5227.1098, 1995.

Choi, Y., Vay, S. A., Vadrevu, K. P., Soja, A. J., Woo, J.-H., Nolf, S. R., Sachse, G. W., Diskin, G. S., Blake, D. R., Blake, N. J., Singh, H. B., Avery, M. A., Fried, A., Pfister, L., and Fuelberg, H. E.: Characteristics of the atmospheric CO_2 signal as observed over the conterminous United States during INTEX-NA, J. Geophys. Res., 113, D07301, doi:10.1029/2007JD008899, 2008.

Denning, A. S., Zhang, N., Yi, C., Branson, M., Davis, K., Kleist, J., and Bakwin, P.: Evaluation of modeled atmospheric boundary layer depth at the WLEF tower, Agr. Forest Meteorol., 148, 206–215, 2008.

Eneroth, K., Kjellström, E., and Holmén, K.: Interannual and seasonal variations in transport to a measuring site in western Siberia and their impact on the observed atmospheric CO_2 mixing ratio, J. Geophys. Res., 108, D214660, doi:10.1029/2002JD002730, 2006.

Fan, S., Gloor, M., Mahlman, J., Pacala, S., Sarmiento, J., Takahashi, T., and Tans, P.: A Large Terrestrial Carbon Sink in North America Implied by Atmospheric and Oceanic Carbon Dioxide Data and Models, Science, 282, 442, doi:10.1126/science.282.5388.442, 1998.

Font, A., Morgui, M. J., and Rodo, X.: Atmospheric CO_2 in-situ measurements: two examples of Crown Design flights in NE Spain, J. Geophys. Res., 113, D12308, doi:10.1029/2007JD009111, 2008.

Geels, C., Gloor, M., Ciais, P., Bousquet, P., Peylin, P., Vermeulen, A. T., Dargaville, R., Aalto, T., Brandt, J., Christensen, J. H., Frohn, L. M., Haszpra, L., Karstens, U., Rödenbeck, C., Ramonet, M., Carboni, G., and Santaguida, R.: Comparing atmospheric transport models for future regional inversions over Europe - Part 1: mapping the atmospheric CO_2 signals, Atmos. Chem. Phys., 7, 3461–3479, 2007, http://www.atmos-chem-phys.net/7/3461/2007/.

Gerbig, C., Lin, J. C., Wofsy, S. C., Daube, B. C., Andrews, A. E., Stephens, B. B., Bakwin, P. S., and Grainger, C. A.: Toward constraining regional-scale fluxes of CO_2 with atmospheric observations over a continent: 1. Observed spatial variability from airborne platforms, J. Geophys. Res., 108(D24), 4756, doi:10.1029/2002JD003018, 2003a.

Gerbig, C., Lin, J. C., Wofsy, S. C., Daube, B. C., Andrews, A. E., Stephens, B. B., Bakwin, P. S., and Grainger, C. A.: Toward constraining regional-scale fluxes of CO_2 with atmospheric observations over a continent: 2. Analysis of COBRA data using a receptor-oriented framework, J. Geophys. Res., 108(D24), 4757, doi:10.1029/ 2003JD003770, 2003b.

Gerbig, C., Körner, S., and Lin, J. C.: Vertical mixing in atmospheric tracer transport models: error characterization and propagation, Atmos. Chem. Phys., 8, 591–602, 2008, http://www.atmos-chem-phys.net/8/591/2008/.

Gerbig, C., Dolman, A. J., and Heimann, M.: On observational and modelling strategies targeted at regional carbon exchange over continents, Biogeosciences, 6, 1949–1959, 2009, http://www.biogeosciences.net/6/1949/2009/.

Gloor, M., Bakwin, P., Hurst, D., Lock, L., Draxler, R., and Tans, P.: What is the concentration footprint of a tall tower?, J. Geophys. Res., 106(D16), 17831–17840, 2001.

Gurney, K. R., Baker, D., Rayner, P., and Denning, S.: Interannual variations in continental-scale net carbon exchange and sensitivity to observing networks estimated from atmospheric CO_2 inversions for the period 1980 to 2005, Global Biogeochem. Cy., 22, GB3025, doi:10.1029/2007GB003082, 2008.

Huang, S., Tu, J., Liu, H., Hua, M., Liao, Q., Feng, J., Weng, Z., and Huang, G.: Multivariate analysis of trace element concentrations in atmospheric deposition in the Yangtze River Delta, East China, Atmos. Environ., 43, 5781–5790, 2009.

Kobayashi, S.: Heterogenity Ratio: a measure of beta-diversity and its use in community classification, Ecol. Res., 2, 101–111, 1987.

Lafont, S., Kergoat, L., Dedieu, G., Chevillard, A., Karstens, U., and Kolle, O.: Spatial and temporal variability of land CO_2 fluxes estimated with remote sensing and analysis data over western Eurasia, Tellus, 54B, 820–833, 2002.

Lin, J. C., Gerbig, C., Wofsy, S. C., Andrews, A. E., Daube, B. C., Grainger, C. A., Stephens, B. B., Bakwin, P. S., and Hollinger, D. Y.: Measuring fluxes of trace gases at regional scales by Lagrangian observations: Application to the CO_2 Budget and Rectification Airborne (COBRA) study, J. Geophys. Res., 109, D15304, doi:10.1029/2004JD004754, 2004.

Liu, S. C. and McAfee, J. R.: Radon 222 and tropospheric vertical transport, J. Geophys. Res., 89(D5), 7291–7297, 1984.

Lloyd, J., Francey, R. J., Mollicone, D., Raupach, M. R., Sogachev, A., Arneth, A., Byers, J. N., Kelliher, F. M., Rebmann, C., Valentini, R., Wong, S.-C., Bauer, G., and Schulze, E.-D.: Vertical profiles, boundary layer budgets, and regional flux estimates for CO_2, and its 13C/12C ratio for water vapour above a forest/bog mosaic in central Siberia, Global Biogeochem. Cy., 15, 267–284, 2002.

Marquis, M. and Tans, P.: Carbon Crucible, Science, 320, 460–461, 2008.

Martins, D. K., Sweeny, C., Stirm, B. H., and Shepson, P. B.: Regional surface flux of CO_2 inferred from changes in the advected CO_2 column density, Agr. Forest Meteorol., 149(10), 1674–1685, 2009.

Matross, D., Andrews, A., Pathmathevan, M., Gerbig, C., Lin, J. C., Wofsy, S. C., Daube, B. D., Gottlieb, E. W., Chow, V. Y., Lee, J. T., Zhao, C., Bakwin, P. S., Munger, J. W., and Hollinger, D. Y.: Estimating regional carbon exchange in New England and Quebec by combining atmospheric, ground-based and satellite data, Tellus, 58B, 344–358, 2006.

Overland, J. E. and Preisendorfer, R. W.: A significance test for principal components applied to a cyclone climatology, Mon. Weather Rev., 110, 1–4, 1982.

Rannik, Ü., Aubinet, M., Kurbanmuradov, O., Sabelfeld, K. K., Markkanen, T., and Vesala, T.: Footprint analysis for measurements over a heterogeneous forest, Bound.-Lay. Meteorol., 97, 137–166, 2000.

Peters, W., Jacobson, A. R., Sweeney, C., Andrews, A. E., Conway, T. J., Masarie, K., Miller, J. B., Bruhwiler, L. M. P., Pétron, G., Hirsch, A. I., Worthy, D. E. J., van der Werf, G. R., Randerson, J. T., Wennberg, P. O., Krol, M. C., and Tans, P. P.: An atmospheric perspective on North American carbon dioxide exchange: CarbonTracker, P. Natl. Acad. Sci., 104(48), 18925–18930, 2007.

Peters, W., Krol, M. C., van Der Werf, G. R., Houweling, S., Jones, C. D., Hughes, J., Schaefer, K., Masarie, K. A., Jacobson, A. R., Miller, J. B., Cho, C. H., Ramonet, M., Schmidt, M., Ciattaglia, L., Apadula, F., Heltai, D., Meinhardt, F., Di Sarra, A. G., Piacentino, S., Sferlazzo, D., Aalto, T., Hatakka, J., Ström, J., Haszpra, L., Meijer, H. A. J., van der Laan, S., Neubert, R. E. M., Jordan, A., Rodó, X., Morguí, J. A., Vermeulen, A. T., Popa, E., Rozanski, K., Zimnoch, M., Manning, A. C., Leuenberger, M., Uglietti, C., Dolman, A. J., Ciais, P., Heimann, M., and Tans, P. P.: Seven years of recent net terrestrial carbon dioxide exchange over Europe constrained by atmospheric observations, Global Change Biol., 16(4), 1317–1337, doi:10.1111/j.1365-2486.2009.02078.x, 2009.

Sarrat, C., Noilhan, J., Lacarrère, P., Donier, S., Lac, C., Calvet, J. C., Dolman, A. J., Gerbig, C., Neininger, B., Ciais, P., Paris, J. D., Boumard, F., Ramonet, M., and Butet, A.: Atmospheric CO_2 modeling at the regional scale: Application to the CarboEurope Regional Experiment, J. Geophys. Res., 112, D12105, doi:10.1029/2006JD008107, 2007a.

Sarrat, C., Noilhan, J., Dolman, A. J., Gerbig, C., Ahmadov, R., Tolk, L. F., Meesters, A. G. C. A., Hutjes, R. W. A., Ter Maat, H. W., Pérez-Landa, G., and Donier, S.: Atmospheric CO_2 modeling at the regional scale: an intercomparison of 5 meso-scale atmospheric models, Biogeosciences, 4, 1115–1126, 2007b, http://www.biogeosciences.net/4/1115/2007/.

Sarrat, C., Noilhan, J., Lacarrère, P., Masson, V., Ceschia, E., Ciais, P., Dolman, A., Elbers, J., Gerbig, C., and Jarosz, N.: CO_2 budgeting at the regional scale using a Lagrangian experimental strategy and meso-scale modeling, Biogeosciences, 6, 113–127, 2009, http://www.biogeosciences.net/6/113/2009/.

Schmitgen, S., Geiß, H., Ciais, P., Neininger, B., Brunet, Y., Reichstein, M., Kley, D., and Volz-Thomas, A.: Carbon dioxide uptake of a forested region in southwest France derived from airborne CO_2 and CO measurements in a quasi-Lagrangian experiment, J. Geophys. Res., 109, D14302, doi:10.1029/2003JD004335, 2004.

Seibert, P. and Frank, A.: Source-receptor matrix calculation with a Lagrangian particle dispersion model in backward mode, Atmos. Chem. Phys., 4, 51–63, 2004, http://www.atmos-chem-phys.net/4/51/2004/.

Shashkov, A., Higuchi, K., and Chan, D.: Aircraft profiling of variation of CO_2 over a Canadian Boreal Forest Site: a role of advection in the changes in the atmospheric boundary layer CO_2 content, Tellus, 59B, 234–243, doi:10.1111/j.1600-0889.2006.00237.x, 2007.

ACPD

10, 8103–8134, 2010

Sidorov, K., Sogachev, A., Langendörfer, U., Lloyd, J., Nepomnjashiy, I. L., Vygodskaya, N., Schmidt, M., and Levin, I.: Seasonal variability of greenhouse gases in the lower troposphere above the eastern European Taïga (Syktyvkar, Russia), Tellus, 54B, 735–748, 2002.

Stohl, A. and Thomson, D. J.: A density correction for Lagrangian Particle Dispersion models, Bound.-Lay. Meteorol., 90, 155–167, 1999.

Stohl, A., Eckhardt, S., Forster, C., James, P., and Spichtinger, N.: On the pathways and timescales of intercontinental air pollution transport, J. Geophys. Res., 107(D23), 4684, doi:10.1029/2001JD001396, 2002.

Stohl, A., Forster, C., Eckhardt, S., Spichtinger, N., Huntrieser, H., Heland, J., Schlager, H., Wilhelm, S., Arnold, F., and Cooper, O.: A backward modeling study of intercontinental transport using aircraft measurements, J. Geophys. Res., 108(D12), 4370, doi:10.1029/2002JD002862, 2003.

Stohl, A., Forster, C., Frank, A., Seibert, P., and Wotawa, G.: Technical note: The Lagrangian particle dispersion model FLEXPART version 6.2, Atmos. Chem. Phys., 5, 2461–2474, 2005, http://www.atmos-chem-phys.net/5/2461/2005/.

Tans, P. P., Bakwin, P. S., and Guenther, D. W.: A feasible global carbon cycle observing system: a plan to decipher today's carbon cycle based on observations, Global Change Biol., 2, 309–318, 1996.

Wofsy, S. C., Harriss, R. C., and Kaplan, W. A.: Carbon dioxide in the atmosphere over the Amazon basin, J. Geophys. Res., 93(D2), 1377–1387, 1988.

Table 1. PSI-500-s overlapping percentage between sites belonging to the same crown (intra-crown comparison): annual and seasonal mean and one standard deviation.

	Annual	DJF	MAM	JJA	SON
600 m a.s.l.					
LMU-TRZ-EGA	51±28	59±26	45±30	51±30	48±25
LIN-MEQ-BIN	44±26	47±25	40±25	41±27	48±25
ULL-MR1-MR2	25±27	27±28	27±27	25±29	23±25
1200 m a.s.l.					
LMU-TRZ-EGA	46±31	49±33	43±30	47±33	46±26
LIN-MEQ-BIN	43±27	43±30	39±25	40±26	48±26
ULL-MR1-MR2	21±26	26±27	21±25	15±24	22±29
2500 m a.s.l.					
LMU-TRZ-EGA	38±33	–	41±30	38±33	37±36
LIN-MEQ-BIN	30±30	23±43	27±30	29±27	37±33
ULL-MR1-MR2	14±28	–	17±33	11±22	16±33
4000 m a.s.l.					
LMU-TRZ-EGA	22±40	–	–	22±40	–
LIN-MEQ-BIN	8±19	–	11±22	–	–
ULL-MR1-MR2	16±26	–	–	18±25	18±29

Table 2. Sorensen's Quocient of Similarity for PSI-500-s belonging to different crowns (inter-crown comparison): annual and seasonal mean and one standard deviation. As no similarity values are found for simulations centered at 4000, no results are shown. For further details, read Sect. 3.2.

	Annual	DJF	MAM	JJA	SON
			600 m a.s.l.		
LMU-LIN	5.6±9.6	8.3±11.4	7.8±12.6	1.0±3.6	5.8±8.25.8
LIN-ULL	10.9±16.2	12.6±17.4	6.9±17.7	10.5±12.5	13.4±18.1
ULL-LMU	0.6±3.1	2.0±5.9	0.7±2.4	0	0
			1200 m a.s.l.		
LMU-LIN	4.5±9.5	7.1±12.8	6.1±11.3	0	5.6±8.6
LIN-ULL	10.2±15.2	11.8±16.3	7.4±16.5	12.8±14.2	8.4±15.3
ULL-LMU	0.6±2.7	2.4±5.3	0	0	0
			2500 m a.s.l.		
LMU-LIN	2.0±10.9	0	0	0	9.8±24.0
LIN-ULL	2.9±6.9	0	0	5.1±9.2	1.6±4.1
ULL-LMU	0.4±2.1	0	0	0	1.6±4.1

ACPD
10, 8103–8134, 2010

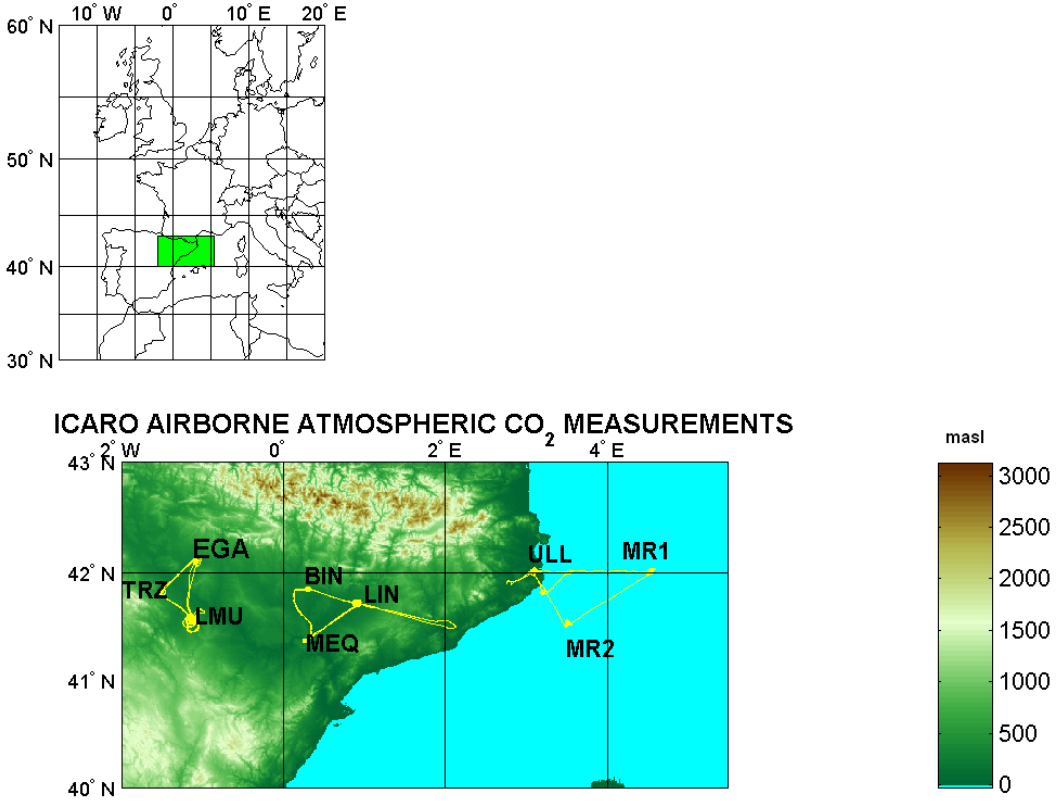

Fig. 1. The network of aircraft sites belonging to the ICARO-II project, in the NE Spain, along parallel 42° N. Topography from the GTOPO30 global Digital Elevation Model (DEM) from the US Geological Survey's EROS Data Center in Sioux Falls, South Dakota; data and documentation available at http://edc.usgs.gov/.

ACPD
10, 8103–8134, 2010

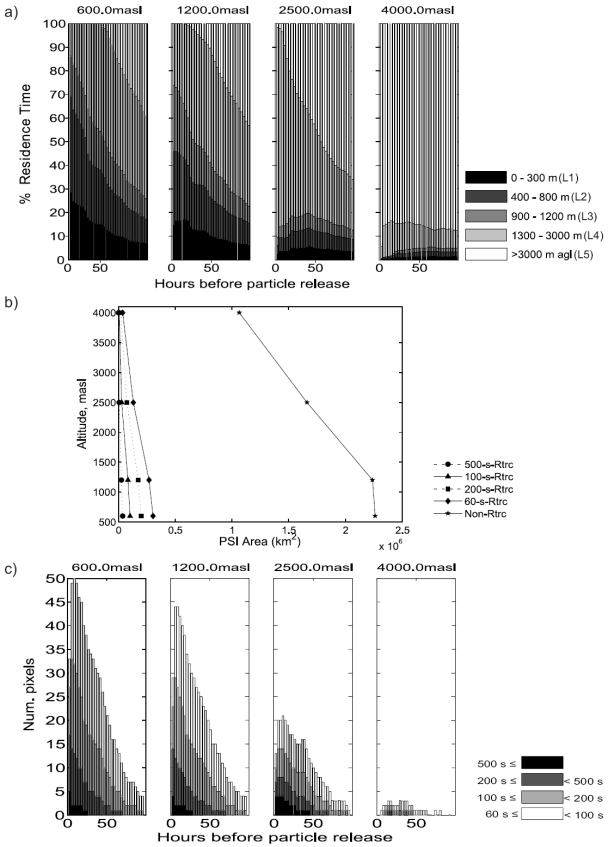

Fig. 2. **(a)** Annual distribution of the percentage of Residence Time (R_t) in different layers of the low troposphere (0–300 or L1, 400–800 or L2, 800–1200 or L3, 1500–3000 or L4 and above 3000 m a.g.l., L5) in time for simulations centered at 600, 1200, 2500 and 4000 m a.s.l. **(b)** Vertical profiles of the annual mean area occupied by the PSI (in km^2) applying different Residence Time Threshold Criteria (R_{ttc} of 500, 200, 100 and 60 s) and without applying any R_{ttc}. c. Number of grid cells belonging to the PSI with R_t higher than 500 s, between 500 and 200 s, between 200 and 100 s and between 100 and 60 s at each time step for each of the releasing altitude (600, 1200, 2500 and 4000 m a.s.l.).

ACPD
10, 8103–8134, 2010

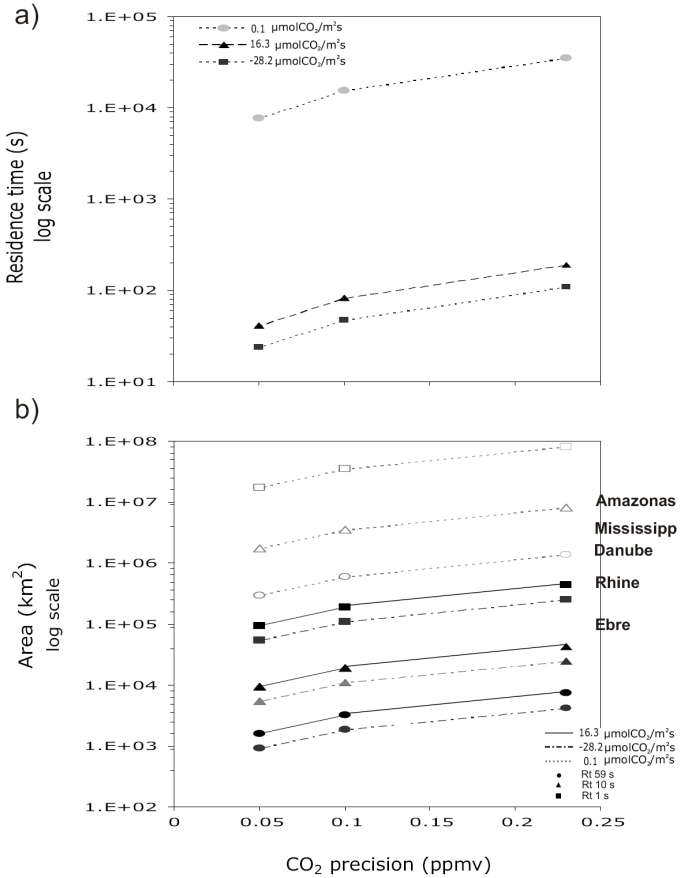

Fig. 3. **(a)** Residence time required to detect changes in the CO_2 mixing ratio in the downstream measurement site by a solely PSI grid cell with CO_2 surface flux values of 16.3, −28.2 and 0.1 µmol CO_2/m^2s. Different precision atmospheric CO_2 analyzers (ppmv) are considered. **(b)** Area occupied by PSI grid cells (km^2) having different R_t values (59, 10 and 1 s) needed to be detected by different precision atmospheric CO_2 analyzers (ppmv). PSI grid cells are supposed to be emitting at the same CO_2 surface flux 16.3, −28.2 and 0.1 µmol CO_2/m^2s. Different river basins areas are pointed to compare the scales of the areas.

ACPD
10, 8103–8134, 2010

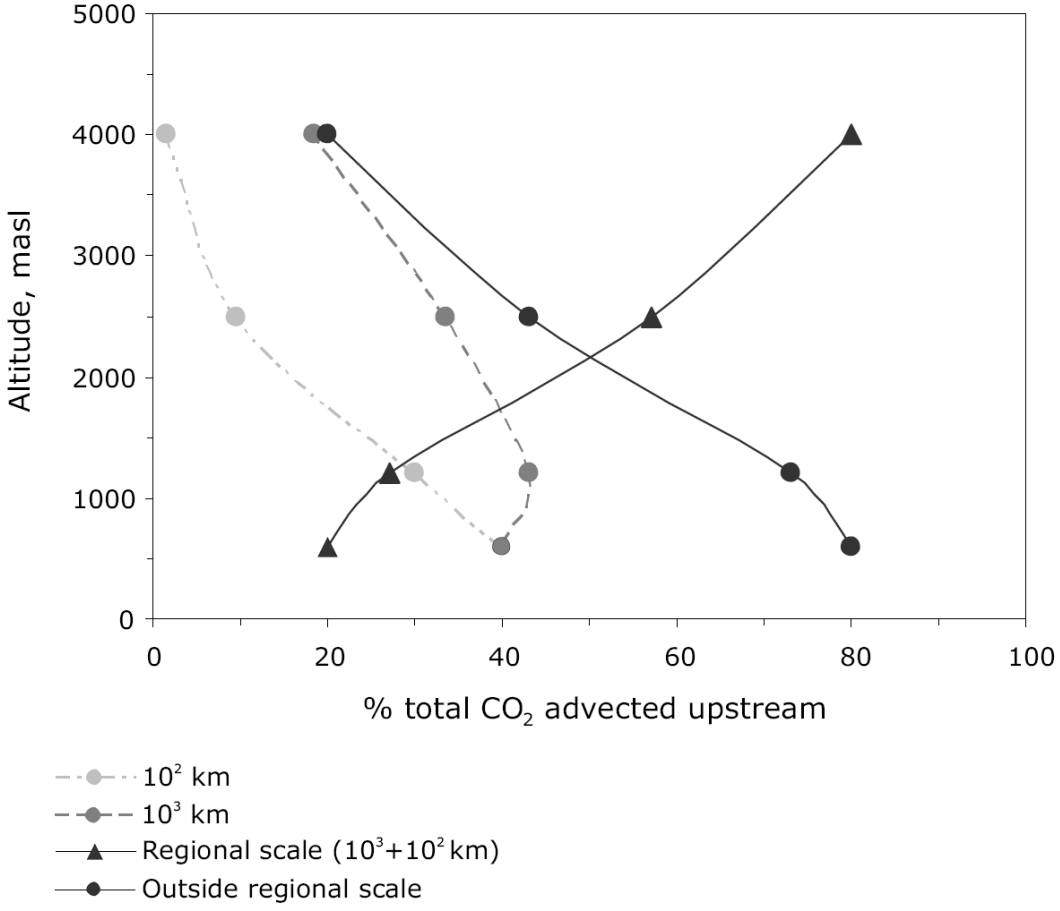

Fig. 4. Vertical distribution of the percentage of the regional surface influence (10^2 and 10^3 km-length) and the outside regional influence (>10^3 km) for the CO_2 vertical profiles belonging to the ICARO-II network of sites.

ACPD
10, 8103–8134, 2010

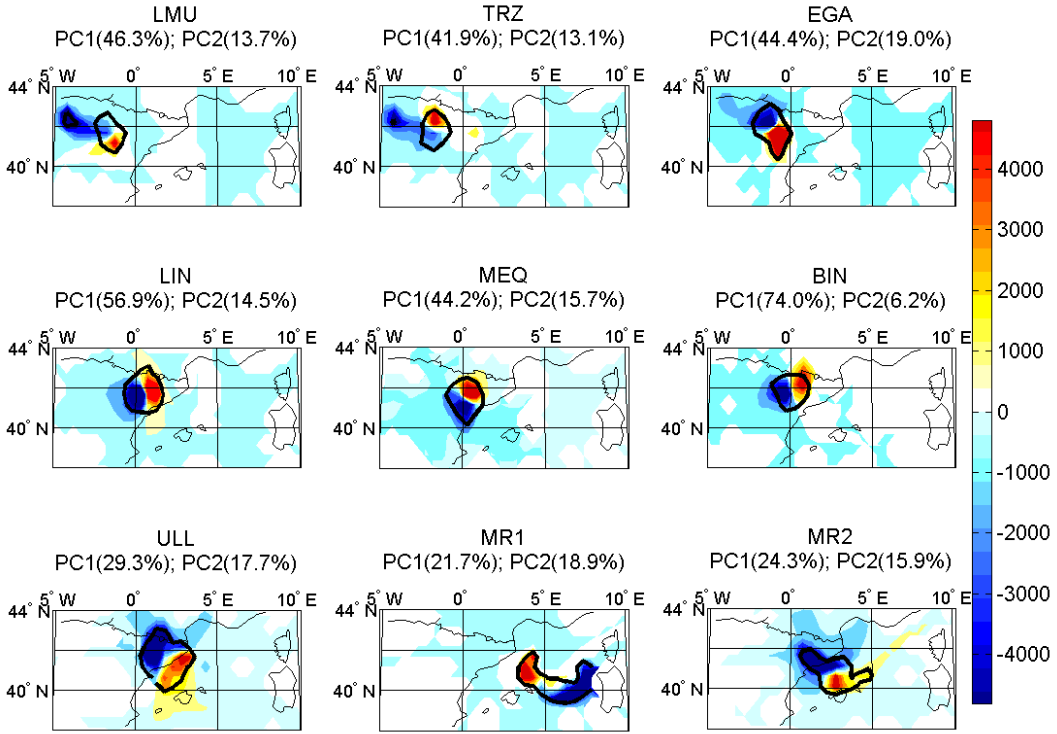

Fig. 5. Maps resulting from Principal Component Analysis (PCA) applied to an original matrix of the residence time in the PSI greater than 500s for each of the nine aircraft measurement sites belonging to ICARO-II. Variables: 51 backward simulations for 2006; observations: residence time in the PSI (applied the 500 s threshold). Distribution of grid cells depending on PC1 and PC2 is shown as the variance explained by each component (percentage with regard to the original variance). Distribution of PSI grid cells due to PC1 is marked with contour black line. Distribution of grid cells due to PC2 is displayed with colored surfaces. PC1 means the most probable regional surface influence of each site. PC2 separates regions with different source of wind marked by synoptic situation.

ACPD
10, 8103–8134, 2010

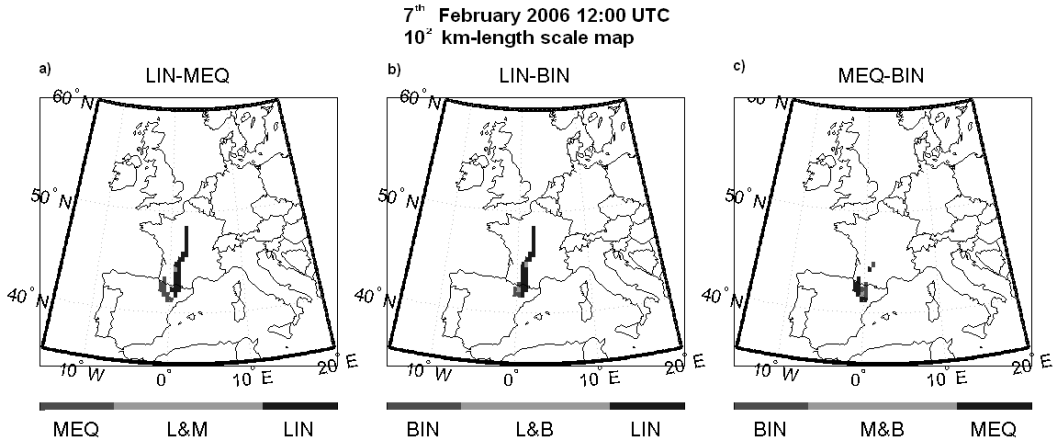

Fig. 6. Pair-by-pair qualitative differences of the Potential Surface Influence (PSI) at 10^2 km-length-scale between LIN, MEQ and BIN for the simulation centered at 12:00 UTC on 7 February 2006. **(a)** LIN and MEQ qualitative differences. **(b)** LIN and BIN qualitative differences. **(c)** MEQ and BIN qualitative differences.

ACPD
10, 8103–8134, 2010

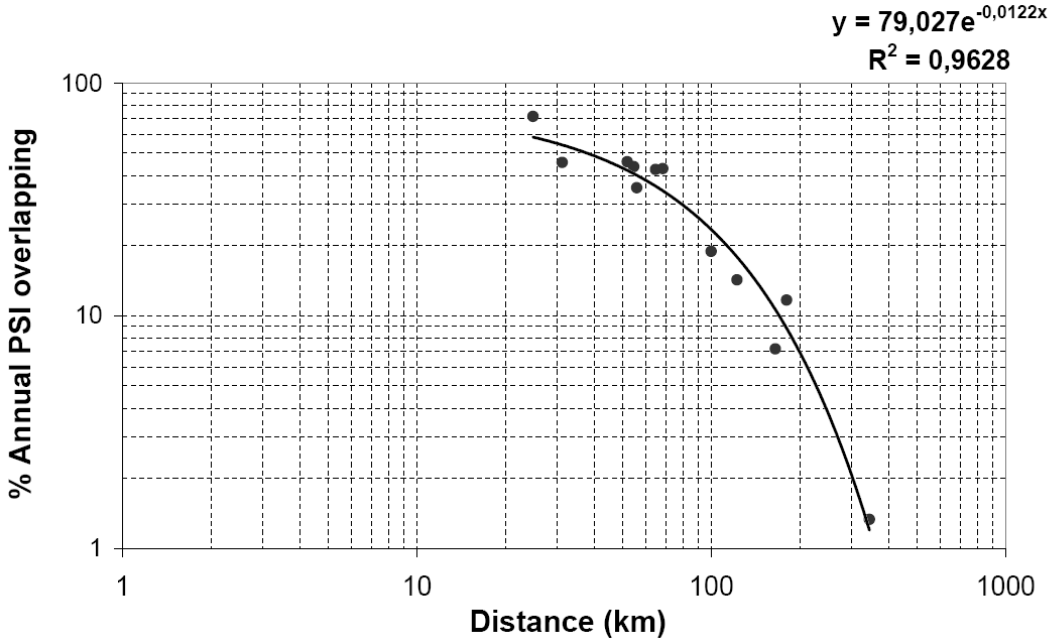

Fig. 7. Annual percentage of overlapping of the PSI area composed by grid cells having R_t>500 s between sites in function of the distance of sites.

ACPD
10, 8103–8134, 2010